Ultrafast Science
A SCIENCE PARTNER JOURNAL

RESEARCH ARTICLE

Ultrashort Isolated Attosecond Pulse Generation with 750-nm Free-Carrier Envelope Phase Near-Infrared Pulses

Xiaowei Wang[1,2†], Fan Xiao[1,2†], Jiacan Wang[1,2], Li Wang[1,2], Bin Zhang[1,2], Jinlei Liu[1,2], Jing Zhao[1,2], and Zengxiu Zhao[1,2*]

[1]Department of Physics, National University of Defense Technology, Changsha 410073, China. [2]Hunan Key Laboratory of Extreme Matter and Applications, National University of Defense Technology, Changsha 410073, China.

*Address correspondence to: zhaozengxiu@nudt.edu.cn
†These authors contributed equally to this work.

Citation: Wang X, Xiao F, Wang J, Wang L, Zhang B, Liu J, Zhao J, Zhao Z. Ultrashort Isolated Attosecond Pulse Generation with 750-nm Free-Carrier Envelope Phase Near-Infrared Pulses. *Ultrafast Sci.* 2024;4:Article 0080. https://doi.org/10.34133/ultrafastscience.0080

Submitted 1 August 2024
Revised 12 November 2024
Accepted 12 November 2024
Published 5 December 2024

Ultrashort laser pulses can serve as fast probes to record instant events. The isolated attosecond pulses (IAPs) generated from high-order harmonic generation (HHG) have been shortened down to about 2 atomic units in time, empowering us to study quantum behaviors of electrons in atoms, molecules, and solids with unprecedented time resolution. Following the cutoff energy law of HHG, the shortest IAP reported so far is driven with short-wavelength infrared (SWIR) pulses, which require additional broadband frequency conversion techniques and raise the bar for attosecond researches. Here, we show that with few-cycle near-infrared (NIR) laser pulses, IAP with pulse duration of 51 ± 4 as is generated during 1-fs linear polarization gate formed by generalized double optical gating (GDOG) technique. The characterization is done with attosecond streak camera, and phase reconstruction is performed with quick phase retrieval by omega oscillation filtering (qPROOF). Furthermore, we show that the IAP generation favors certain carrier envelope phases (CEPs) in the narrow gate, i.e., IAP is only efficiently produced for certain CEPs, which eliminates the requirement of CEP stabilization. The demonstrated scheme for IAP generation in principle has much higher conversion efficiency than the long-wave driver scheme according to the wavelength scaling law of HHG. Our work suggests an alternative way to generate ultrashort IAPs by applying GDOG on few-cycle free-CEP NIR driving pulses, and is thereby of great importance to facilitate the development of attosecond science and technology.

Introduction

Pulsed light, like a flash, exposes the darkness for a fleeting instant, allowing us to record fast repeatable processes frame by frame with pump-probe technique [1,2], with tiny time interval determined by the pulse duration. Laser pulses with duration as short as tens to hundreds of attoseconds [3–6] have been proven to be revolutionary probes to measure the previously believed immeasurable quantum dynamics inside atomic and molecular systems, such as real-time valance electron motion [7,8], the timing of photoemission [9], electronic correlations [10], charge migration [11,12], and so on. However, current applications of isolated attosecond pulse (IAP), i.e., attosecond transient absorption spectroscopy [7,13–15], attosecond beating by interference of 2-photon transitions [16,17], and attosecond streak camera [18,19], usually rely on another light-field-synchronized femtosecond pulse, since it is yet not easy to perform direct attosecond pump-attosecond probe experiments. Therefore, improving the IAP photon flux to enable the absorption of 2 or more IAP photons and shortening the IAP pulse duration to ensure high temporal resolution based on pulse envelope are of critical importance to further unleash the power of IAP on the measurements of ultrafast electron dynamics.

According to the time-energy uncertainty principle, synthesizing of ultrashort IAP would need photons with energy spread of more than tens of electron volts [3,20]. This can be realized via high-order harmonic generation (HHG) [21–23] whose cutoff energy is determined by the ponderomotive energy U_p as $U_p \propto I_L \lambda_L^2$. Therefore, the route to produce ultrashort IAP with broadband spectrum, at first sight of the cutoff energy law, is to employ long wavelength pulses due to the quadratic dependence. Indeed, the shortest IAPs with duration of 43 as [24] and 53 as [25], with cutoff photon energy up to 170 and 330 eV, respectively, are both driven by short-wavelength infrared (SWIR) pulses centered at 1.8 μm. The strategy of adopting longer wavelength driving pulses, leaving aside the additional effort and cost to build SWIR lasers [26,27], is, however, undesirable in the sense of improving the IAP flux, since the conversion efficiency drops dramatically as central wavelength increases [28,29]. Furthermore, although much higher

cutoff energy and even shorter IAPs are expected, SWIR pulses are not necessarily needed for the generation of state-of-the-art near-50-as IAPs from the point of view of enough spectral bandwidth. Broadband extreme ultraviolet (XUV)/soft x-ray spectra supporting Fourier transform (FT) limited pulses with duration of 40 as [30], 32 as [31], 20 as [32], and even 16 as [33] are experimentally demonstrated, of which the mechanism can be understood by revisiting the cutoff energy law at second sight, i.e., increasing the laser intensity instead of central wavelength. Although the pulse energy can be increased up to tens to thousands of millijoules with chirped pulse amplification technique, there exists a saturation intensity set by the full ionization of the target. Therefore, special steps, e.g., compressing the temporal width of driving lasers and/or increasing the ionization potential, should be taken to avoid the ionization saturation effect.

Herein, we demonstrate the generation of ultrashort IAP with temporal full width at half maximum (FWHM) of 51 as with few-cycle NIR pulses centered at 0.75 μm. By taking advantage of generalized double optical gating (GDOG) technique [34,35], which preserves both the plateau and cutoff region photons, the sample ionization by the leading edge of the driving field is greatly suppressed, resulting in high saturation intensity and hence high IAP cutoff energy. Another benefit that comes with GDOG is the needlessness of carrier envelope phase (CEP) stabilization of the driving laser pulses, as experimentally demonstrated previously [36,37]. However, the underlying mechanisms are never uncovered. Here, we numerically show that narrow linear polarization gate formed with GDOG allows effective IAP emitting only from specific laser waveforms with some certain CEPs due to the extremely sensitive dependence of IAP generation on the carrier waveform of the driving laser. This makes for passive ultrabroadband IAP gating with CEP unstabilized driving lasers. This is in contrast to another CEP-irrelevant IAP generation scheme [38], which is based on phase-matching-assisted amplitude gating and keeps only the cutoff spectral components, resulting in longer IAP pulses. The generated IAP is characterized with attosecond streak camera and reconstructed with the quick phase retrieval by omega oscillation filtering (qPROOF) algorithm [39]. This work exhibits the feasibility of the generation of ultrashort attosecond pulses with sophisticated Ti:sapphire driving lasers and thereby holds out the prospect of high-flux and short-duration IAP generation for future attosecond pump-attosecond probe experiments, as demonstrated recently with attosecond pulse trains [40].

Experimental Design

The IAP generation and characterization platform for our experiments was essentially a pump-probe interferometer, as illustrated in Fig. 1. The waveform of linearly polarized NIR pulse was reshaped with GDOG optics to form a narrow gate for isolating IAP. The GDOG optics, as detailed in the inset figure, consist of a 178-μm-thick quartz plate (QP1), a second quartz plate (QP2) with thickness of 445 μm, a 0.5-mm-thick fused silica window (BW) placed with Brewster angle for gating field, and a 141-μm-thick β-barium borate (BBO). The thicknesses of the 4 optics were carefully configured [34] so that the linear gate lasts only for about 1 fs and the polarization direction in the gate is parallel to that of the input pulse. Note that only one fused silica BW was employed to attenuate the driving field, reflecting away only about 30% pulse energy, whereas near 50%

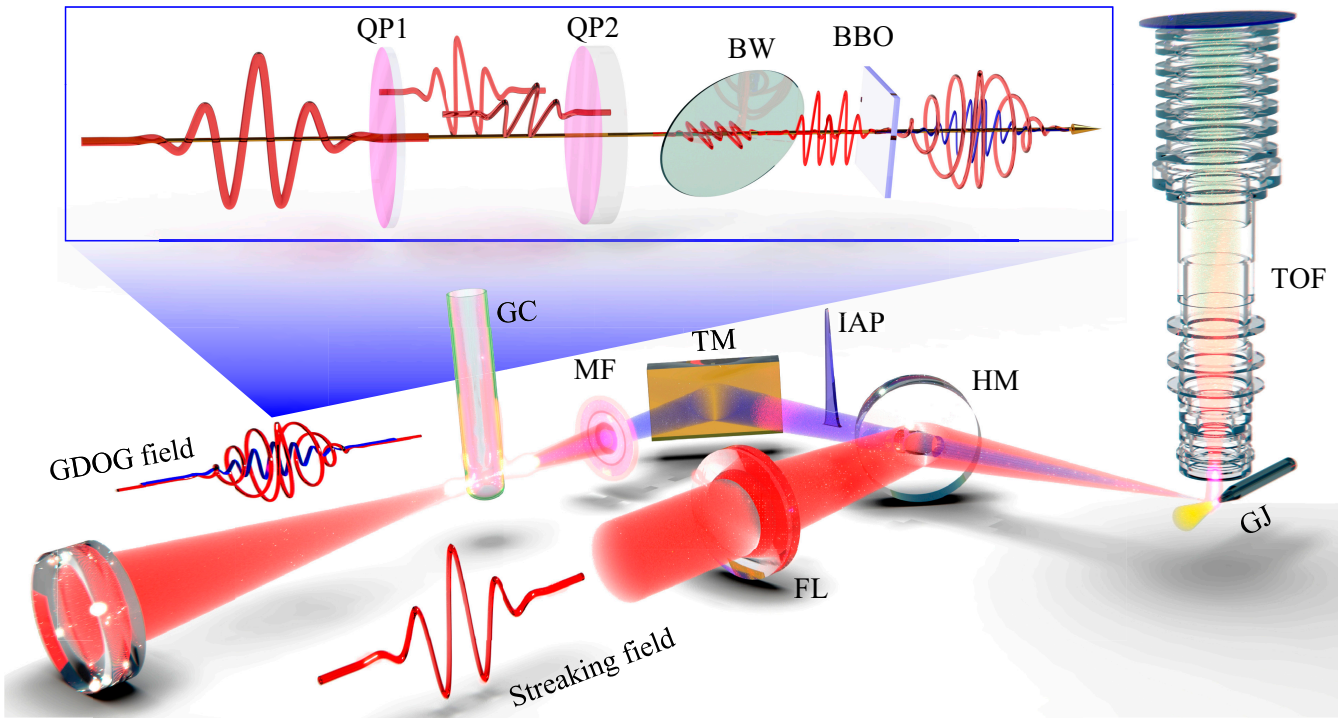

Fig. 1. The schematic of the experimental setup. The IAP was generated in a neon-filled gas cell (GC) with GDOG field. The IAP intrinsic dispersion was compensated with a 200-nm-thick Zr metal foil (MF), with which the residual NIR pulses were blocked as well. The IAP and streaking fields were then recombined with a hole-drilled mirror (HM) and focused by a toroidal mirror (TM) and a focusing lens (FL), respectively, onto a neon gas jet (GJ). The modulated energy spectra of the electron bunch were then measured by a time-of-flight (TOF) spectrometer. The GDOG field was generated with GDOG optics that consist of 2 quartz plates (QP1 and QP2), a Brewster window (BW), and a β-barium borate (BBO), as shown in the inset figure.

pulse energy was thrown away in the standard GDOG scheme [34]. The reason for keeping higher driving pulse energy was that high peak laser intensity was desired for extending the cutoff energy. The laser fields were then focused by a spherical silver mirror ($f = 350$ mm) into neon-filled gas cell (GC), reaching high laser intensities up to 4 PW/cm^2 (10) (1 PW = 1×10^{15} W), to generate IAP. Zirconium (Zr) metal foil (MF) with thickness of 200 nm was used to block the residual NIR pulses and compensate the intrinsic atto-chirp. Toroidal mirror ($f = 270$ mm) was used to image the attosecond source onto a neon gas jet (GJ) with 2f-2f geometry. In the meantime, another focused replica of the NIR pulse termed as streaking field was recombined with the IAP pulse by a hole-drilled silver mirror (HM). The energy spectra of the electron bunch created during the single-photon ionization of neon atoms by IAP field were modulated by the streaking field and measured as a function of IAP-NIR delay by a time-of-flight (TOF) spectrometer. The streaking trace is obtained, from which the temporal profile of IAP can be extracted with various algorithms [41–48].

Before the experiments, we need to look into the NIR laser field in detail, since the generation of IAP in the HHG process occurs in the sub-laser-cycle time scale so that the electric waveform instead of the pulse envelope of driving pulse matters. We start with the electric field of a short laser pulse described as $E(t) = A(t)cos\left(\omega_L t + \phi_{CEP}\right)$, with $A(t)$ being a gaussian envelope, ω_L being the central angular frequency, and ϕ_{CEP} being the CEP phase. Special attentions should be paid to the dispersion introduced by the GDOG optics since ultrashort NIR pulses are dealt with in the experiments. Significant temporal broadening can be introduced during the propagation in GDOG optics. To accommodate this, the input pulse is first precompensated to have about −70 fs^2 group delay dispersion (GDD). The propagation in the GDOG optics is then simulated. After QP1, the o-ray and e-ray are separated by integral multiple (2) optical cycles so that their projections on the polarization plane of the input pulse add up constructively, forming the so-called driving field. In the orthogonal plane, they cancel each other out in the overlapping center, forming the gating field, as shown in Fig. 2A. QP2 is used to introduce additional 5-cycle delays, as shown in Fig. 2B. To improve the gating effect, the relative field strength of the gating field is enlarged by reflecting off 30% of the driving field with the BW. Afterward, the second harmonic of the gating field, with polarization parallel to the driving field, is produced in the BBO with type-I phase matching. An asymmetric driving field is then synthesized, as shown in Fig. 2C. More importantly, the driving field, which is the e-ray in BBO, caught up with the gating field (o-ray), resulting in a quarter-wave phase retardation between the 2 components. The leading edge and trailing edge are then circularly polarized, while the central part remains linearly polarized since the gating field vanished in the center. It is worth noting that the driving field is comparable or even slightly higher than the gating field in the leading and trailing edge, which is inconsistent with the standard GDOG scheme. It is caused by the lower attenuation factor of BW and by incorporating the material dispersion and the second harmonic in the simulation. However, the key point of GDOG, i.e., reducing the delay between the gating and driving pulses, is realized by the insertion of the BW. Due to the

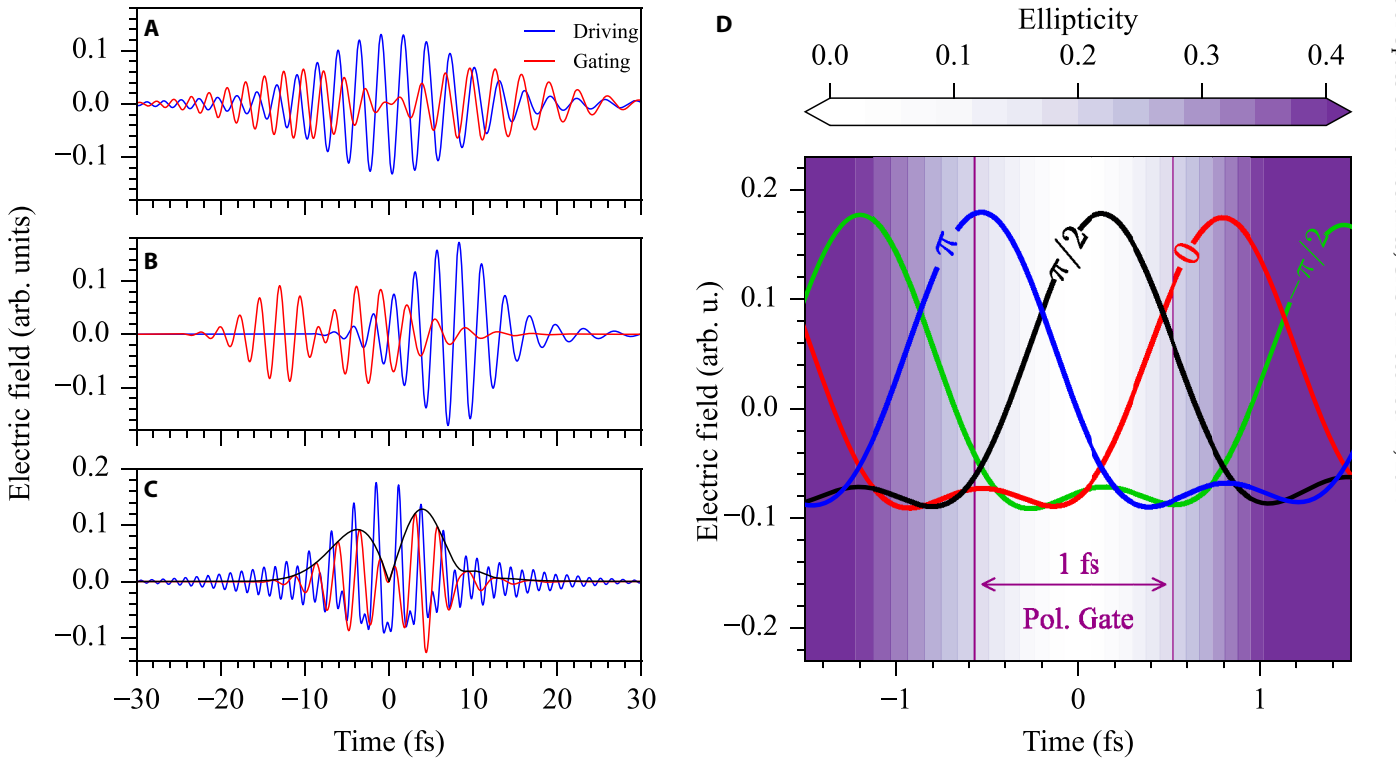

Fig. 2. The formation of driving and gating fields with GDOG optics. (A) The linearly polarized input pulse is split by a birefringence crystal (QP1) as the driving (blue) and gating (red) fields. (B) Additional phase retardation between them is introduced by QP2. (C) The driving field is further attenuated by a Brewster window and desymmetrized by the second harmonic of the gating field with a BBO crystal. The relative delay between the 2 orthogonal components, meanwhile, is adjusted to be a quarter wave, leading to polarization gating fields. (D) The contours show time-dependent ellipticity and define a 1-fs polarization gate (Pol. Gate), in which the ellipticity is smaller than 0.2. The waveforms of the driving field for CEP of $-\pi/2$ (green), 0 (red), $\pi/2$(black), and π (blue) show critical difference in the gate.

pre-introduced negative chirp of the input pulse, the gating and driving fields get shorter and shorter during their propagation in the optics. The ellipticity ϵ, i.e., the ratio of the gating pulse intensity to the driving pulse intensity, varies rapidly as time, as contoured in Fig. 2D. Time zero corresponds to $\epsilon = 0$, and the 2 vertical lines ($\epsilon = 0.2$) roughly define the temporal window (1 fs) for IAP generation.

Although the gate width is determined by GDOG optics, the waveform of the driving field inside the gate is subjected to change as the CEP of input pulse changes. Four electric fields corresponding to CEPs of $-\pi/2$ (green), 0 (red), $\pi/2$(black), and π (blue) are shown in Fig. 2D. Note that the time-dependent ellipticity remains the same for different CEPs, since the pulse envelopes of both fields are immune to CEP. It is shown that as CEP increases, the driving field shifts toward earlier time with marginal change of peak field strength, exposing different part of the waveform in the linear polarization window. The emission of IAP is consequently altered. According to the 3-step model, electrons tunneled after the electric field peak contribute to IAP emission, and those liberated before the peak are driven away from the ion. Therefore, it can be asserted that the waveforms with CEPs of $-\pi/2$ and zero generate no significant amount of IAP photons, assuming that the negative electric field is weak enough. For the CEP of π, the electron would spend most of its excursion time in the linear polarization field; it is thus more favorable than the case of $\pi/2$. Although many qualitative analysis can be drawn, it is necessary to perform numerical simulations to quantify the CEP dependence of IAP yields, spectra, and phases so that optima CEPs, if exist, can be found for ultrashort IAP generation.

Results and Discussion

The simulations were carried out by solving the 2-dimensional time-dependent Schrödinger equation (2D-TDSE) with single active electron (SAE) approximation. During the real-time propagation, an absorbing boundary was applied to prevent the unphysical reflection from the boundary. The size of the simulation box was tuned to exclude the long trajectories of the recombining electrons, so only short trajectory contributions were taken into account, which can be experimentally realized through phase matching. The dipole spectra were filtered by the transmission of Zr foil, and the electric field of IAP was obtained via the inverse FT of the spectra. The peak intensity of the input pulse was set to be 2.5 PW/cm^2, resulting in about 1.0 PW/cm^2 driving field due to the energy transfer to gating field and attenuation by BW. The numerical results show that only one attosecond pulse survives from the ellipticity-varying laser field for all the CEP values, as shown in Fig. 3A. However, the calculated yields of IAPs show sensitive CEP dependence, as shown in Fig. 3B. The IAP yield reaches its maximum around a CEP value of 193 deg, away from which the IAP yield drops quickly, suggesting a CEP window from 135 deg to 255 deg for effective IAP generation. It should be pointed out that the CEP used in the simulation is the CEP of the input pulse before the

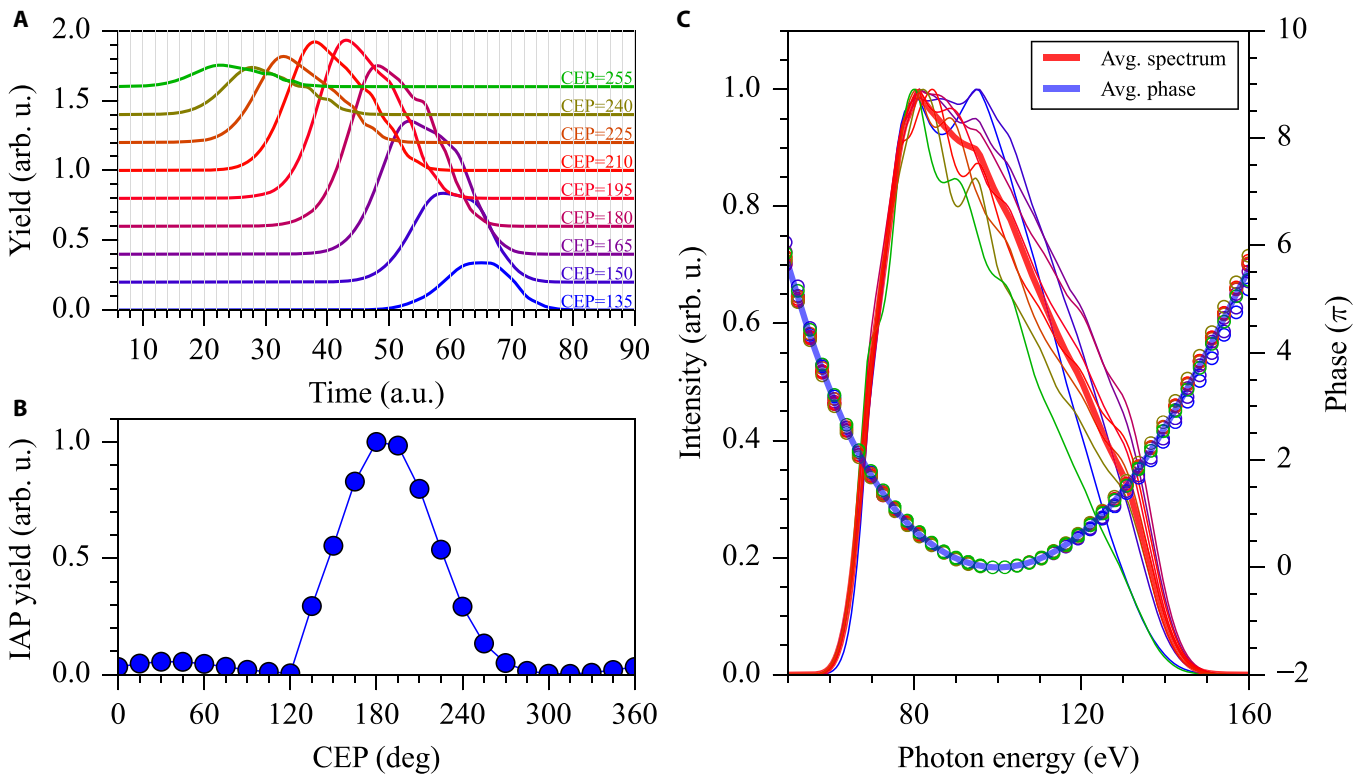

Fig. 3. The influence of CEP on IAP generation investigated with 2D-TDSE. (A) The yields of IAP corresponding to laser CEP from 135 to 255 deg exhibit strong CEP dependence, whereas the temporal width has subtle change for different CEPs. (B) The IAP yield maximizes at CEP between 180 to 195 deg and drops by an order of magnitude when CEP changes by 60 deg from the maximum position. (C) 2D-TDSE calculated spectra (colored thin lines) and spectral phase (hollow circles, with the zeroth and the first order being removed) of the IAPs. The thick red line is the average spectrum, and the thick blue line is the averaged phase. For IAPs generated with CEP from 135 to 255 deg beyond which the IAP yield is marginal, the spectral profile and phase are quite similar, which makes it possible to produce IAPs without CEP stabilization. Note that the CEP values should only be referred relatively. Their absolute values are meaningless since the propagation in air and optical window is not taken into account.

GDOG optics, and it should only be referred relatively. Its absolute value is meaningless since the propagation in air and optical window is not included. The simulation implies that CEP stabilization is no longer indispensable to produce an IAP, which was experimentally demonstrated before [36] for narrow-band long-lasting IAPs, and it still remains questionable if the pulse duration changes with CEP and if the scheme can be employed for ultrashort IAP generation.

As shown in Fig. 3A, the durations of IAPs are evaluated to be around 359 as, with a standard deviation of 20 as, despite different absolute emission times. The IAPs are temporally stretched due to the intrinsic atto-chirp and can be further compressed with material dispersion [49–52]. However, whether the IAPs for different CEP values can be satisfactorily compensated simultaneously depends on whether their spectra and phase are the same. We focus only on the stronger IAPs for driving laser CEP between 135 and 255 deg, beyond which the IAP flux drops by an order of magnitude. In Fig. 3C, the normalized spectra (colored thin lines) and phases (hollow circles) of the IAPs shown in Fig. 3A are compared. Note that the low-energy photons below 50 eV were removed by Zr transmission window and that the zeroth and first order of the phases are artificially removed. The results show roughly the same spectral profiles and phase variations, implying that they have and will always keep similar temporal profiles during the propagation in any dispersive materials used in experiments. Therefore, the gating and pulse duration of IAPs can both be considered as CEP independent.

In the experiments, the laser intensity of 5-fs pulses centered at 750 nm was adjusted to be in the vicinity of that in the simulations, i.e., 2.5 PW/cm^2, to keep the photon energy below 150 eV, since the Zr MF has negative GDD in this region [5,20,37]. With the streaking camera, electron spectrogram, as shown in Fig. 4A, was measured in a delay range of 10.9 fs with a step size of 211 as. Although the scanning is not performed for the entire persistent period of the NIR streaking pulses and results in an asymmetric trace, it has been demonstrated that streaking traces with few-laser-cycle oscillations are sufficient to retrieve the attosecond pulses with either PROOF [25,39] or VTGPA (Volkov-transform generalized projection algorithm) [24,44] technique. The oscillation of the streaking trace lasts much longer than the claimed 5-fs pulse width, indicating the existence

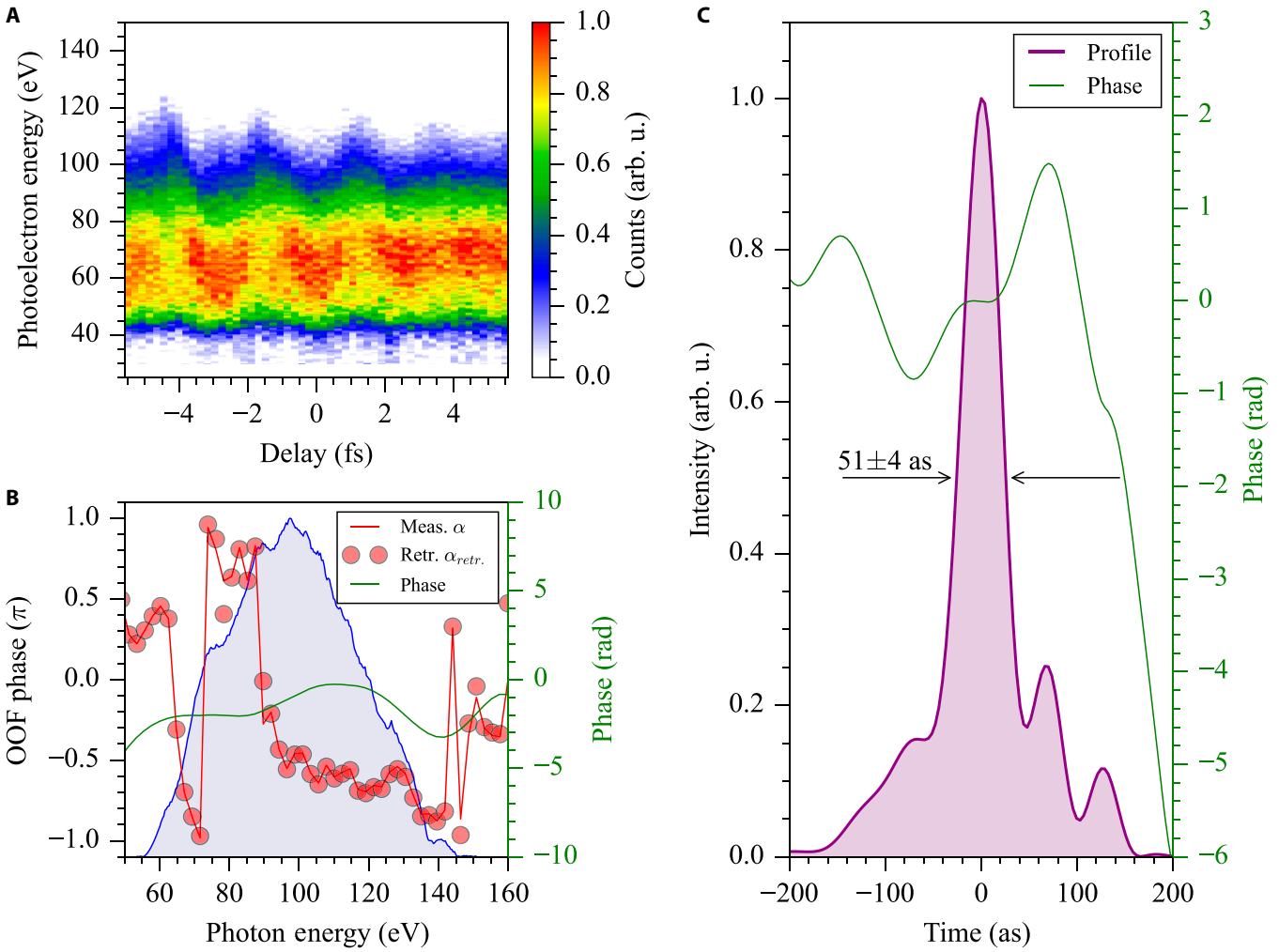

Fig. 4. The reconstruction of isolated 51-as IAP. (A) Streaking trace measured as the NIR pulse-modulated photoelectron spectra as a function of IAP-NIR delay. The delay step size is 211 as, with time jitter of 25 as. (B) Retrieved spectra phase (green line) with the qPROOF algorithm. The retrieved OOF phases (circles) consist of the extracted ones (red line) from the streaking trace, indicating a successful phase retrieval. The spectra profile of the IAP is shown in shaded area. (C) The temporal profile with FWHM of 51 (± 4) as is obtained by performing inverse FT with the retrieved spectral phase and the measured spectral profile. The temporal phases (green line) are also obtained. There exists a long-lasting structure in the profile, which can be attributed to the remaining high-order phase dispersions.

of pedestals in the ultrashort streaking pulses due to nonperfect dispersion compensation. During the change of NIR-IAP delay, the photoelectron spectrum is modulated repeatedly in every laser cycle; therefore, one-cycle scanning can theoretically encode all the IAP phase information. Since the CEP was not stabilized, the electron count rate was pretty low, and each spectrum was taken by integrating 50,000 laser shots. The pump-probe time delay was actively stabilized [53] and measured to have root-mean-square time jitter of ~25 as [14].

The reconstruction of the IAP is in nature a phase retrieval problem, which was solved with the qPROOF algorithm. The qPROOF algorithm first extracted the phase of the one omega frequency (OOF) components, shown as the red line in Fig. 4B, following the same procedure in PROOF. Then, the spectral phases of IAP, shown as the green line in Fig. 4B, were then solved iteratively with analytical derivatives, whereas the same problem was solved with genetic algorithm in PROOF. Therefore, the qPROOF algorithm converges much faster than and has the same logic as PROOF that has been tested for short [5] and ultrashort [25] IAP characterization. The solved OOF phases, shown as the red circles in Fig. 4B, matched the measured ones, and result in a retrieval error [39] of 0.625, indicating a successful retrieval. The principle of measuring IAPs with unstabilized CEP laser pulses lies in 2 facts [36]: (a) The IAP is locked to the electric field, rather than the envelope, of the driving laser; (b) the temporal profile and phase of the IAPs do not change significantly as CEP changes, as demonstrated above.

The IAP continuous spectrum (solid line with filled area) shown in Fig. 4B is obtained from the streaking-field-free electron spectrum by taking into account both the ionization potential shifting and nonflat ionization cross section of Ne atoms. The spectrum, together with the retrieved spectral phase, is used to reconstruct the electric field $E_X(t)$ of IAP, whose intensity profile (solid line with filled area) and temporal phase (green solid line) are shown in Fig. 4C. The FWHM of the IAP is thus determined to be 51 ($\pm$ 4) as. However, the IAP has a wide structure that lasts for 400 as due to the remaining high-order dispersion, which is located mainly in the energy range of 90 to 110 eV and 120 to 140 eV. New dispersion management techniques other than the insertion of MF will be needed to further compensate the remaining dispersion. The uncertainty of the pulse duration of the measured IAP comes from 3 parts. The first one is caused by the qPROOF algorithm; with the experimental parameters, i.e., 1 TW/cm^2 (1 TW = 1×10^{12} W) and 5-fs streaking pulses, the algorithm is determined numerically to have a retrieval error of $\Delta\tau_1 = 3$ as. The second one is attributed to the intensity stability of the laser system, which causes the change of IAP spectra width. By monitoring the IAP spectra change for 2 h, the supporting IAPs have a duration change of $\Delta\tau_2 = 1$ as. The last one comes from the small IAP spectra difference for different CEPs as shown in Fig. 3C. The weight-average results in another error $\Delta\tau_3 = 1$ as. The total duration uncertainty is thus estimated as $\Delta\tau = \sqrt{\Delta\tau_1^2 + \Delta\tau_2^2 + \Delta\tau_3^2} \approx$ 4 as. On the other hand, other experimental parameters, e.g., 25 as time jitter, 211 as step size, and 4.5% noise level, contribute little in the retrieval error according to previous numerical simulations [39].

The avoidance of CEP stabilization will greatly ease the generation of ultrashort IAPs. More importantly, the resulted IAPs are always locked to the NIR drivers and are hence still suitable for IAP-NIR pump-probe measurements. However, the stabilization of CEP is still a better choice in the case that intense IAPs are needed. With stabilized CEP, the yield of IAP can be improved by 4 times, which is determined as the ratio of the maximum to the average for CEP-dependent IAP yield shown in Fig. 3B. Therefore, free-CEP drivers are adequate for one XUV-photon-related linear measurements, while CEP stabilization is needed for high-flux IAP generation. On the other hand, using NIR pulses, which have higher theoretical conversion efficiency, is also capable of producing broadband ultrashort IAPs. The demonstrated 51-as pulses can be further shortened with wider GDD compensation window, such as 33-as IAPs from NIR drivers, which are predicted with C filter as the compensation material [20]. With slightly longer wavelength drivers, the cutoff can even be extended up to 5.2 keV [54], or the average power can be improved to be 5.1 μW [55]. Therefore, high-flux IAPs with ultrashort pulse duration can be generated with CEP unstabilized shorter wavelength drivers.

Conclusion

In conclusion, we demonstrate 51-as IAP generation with CEP unstabilized few-cycle NIR driving pulses. The drawback of short-wavelength driver on extending the bandwidth is remedied by the increased saturation intensity associated with the short driving pulse duration and decreased ionization in the leading edge associated with GDOG technique. We show that by setting a narrow gating window, broadband IAPs can be emitted regardless of the CEP. Furthermore, the intrinsic attochirp of IAPs for various CEPs is identical and can be compensated by a Zr foil. The temporal characterization of IAP was carried out with attosecond streak camera, and the phase retrieval was done with qPROOF algorithm. The highlight of this work is to use GDOG scheme with few-cycle NIR driving pulses, which ensures high saturation intensity and generates ultrashort IAP with pulse duration comparable to that with SWIR drivers. It therefore holds the promise of generating high-flux ultrashort IAPs so as to popularize and expand the application of attosecond pulses.

Acknowledgments

Author contributions: X.W. and Z.Z. conceived the idea. Z.Z. supervised the project. X.W., F.X., and L.W. developed the experimental setup. X.W., F.X., and J.W. performed the experiments. F.X. and J.W. performed the phase retrieval. X.W., B.Z., J.Z., J.L., and Z.Z. performed the 2D-TDSE simulations. X.W., F.X., and Z.Z. wrote the manuscript. All authors contributed to the discussion of the manuscript.

Funding: This work was supported by the National Key Research and Development Program of China (grant no. 2019YFA0307703), the Major Research Plan of the National Natural Science Foundation of China (grant no. 91850201), and the National Natural Science Foundation of China (grant nos. 12234020 and 11974426).

Competing interests: The authors declare that they have no competing interests.

Data Availability

The data that support the findings of this study are available from the corresponding authors upon reasonable request.

Supplementary Materials

Supplementary Text
Reference [56]

References

1. Zewail AH. Femtochemistry: Atomic-scale dynamics of the chemical bond. *J Phys Chem A*. 2000;104(24):5660–5694.
2. Bhattacharjee Y. Measuring the immeasurable. *Nature*. 2001;412:474–476.
3. Midorikawa K. Progress on table-top isolated attosecond light sources. *Nat Photonics*. 2022;16:267–278.
4. Li J, Lu J, Chew A, Han S, Li J, Wu Y, Wang H, Ghimire S, Chang Z. Attosecond science based on high harmonic generation from gases and solids. *Nat Commun*. 2020;11:2748.
5. Zhao K, Zhang Q, Chini M, Wu Y, Wang X, Chang Z. Tailoring a 67 attosecond pulse through advantageous phase-mismatch. *Opt Lett*. 2012;37(18):3891–3893.
6. Zhong S, Teng H, Zhu X, Gao Y, Wang K, Wang X, Wang Y, Yu S, Zhao K, Wei Z. Characterizing 86-attosecond isolated pulses based on amplitude gating of high harmonic generation [Invited]. *Chin Opt Lett*. 2023;21(11):Article 113201.
7. Goulielmakis E, Loh ZH, Wirth A, Santra R, Rohringer N, Yakovlev VS, Zherebtsov S, Pfeifer T, Azzeer AM, Kling MF, et al. Real-time observation of valence electron motion. *Nature*. 2010;466:739–743.
8. Chini M, Wang X, Cheng Y, Wu Y, Zhao D, Telnov DA, Chu S-I, Chang Z. Sub-cycle oscillations in virtual states brought to light. *Sci Rep*. 2013;3:1105.
9. Schultze M, Fieß M, Karpowicz N, Gagnon J, Korbman M, Hofstetter M, Neppl S, Cavalieri AL, Komninos Y, Mercouris T, et al. Delay in photoemission. *Science*. 2010;328(5986): 1658–1662.
10. Ossiander M, Siegrist F, Shirvanyan V, Pazourek R, Sommer A, Latka T, Guggenmos A, Nagele S, Feist J, Burgdörfer J, et al. Attosecond correlation dynamics. *Nat Phys*. 2017;13:280–285.
11. Calegari F, Ayuso D, Trabattoni A, Belshaw L, de Camillis S, Anumula S, Frassetto F, Poletto L, Palacios A, Decleva P, et al. Ultrafast electron dynamics in phenylalanine initiated by attosecond pulses. *Science*. 2014;346(6207):336–339.
12. Matselyukh DT, Despré V, Golubev NV, Kuleff AI, Wörner HJ. Decoherence and revival in attosecond charge migration driven by non-adiabatic dynamics. *Nat Phys*. 2022;18:1206–1213.
13. Wang H, Chini M, Chen S, Zhang C-H, He F, Cheng Y, Wu Y, Thumm U, Chang Z. Attosecond time-resolved autoionization of argon. *Phys Rev Lett*. 2010;105(14):Article 143002.
14. Wang L, Bai G, Wang X, Zhao J, Gao C, Wang J, Xiao F, Tao W, Song P, Qiu Q, et al. Raman time-delay in attosecond transient absorption of strong-field created krypton vacancy. *Nat Commun*. 2024;15(1):2705.
15. Di Palo N, Inzani G, Dolso GL, Talarico M, Bonetti S, Lucchini M. Attosecond absorption and reflection spectroscopy of solids. *APL Photonics*. 2024;9:Article 020901.
16. Paul PM, Toma ES, Breger P, Mullot G, Augé F, Balcou P, Muller HG, Agostini P. Observation of a train of attosecond pulses from high harmonic generation. *Science*. 2001;292(5522):1689–1692.
17. Gong X, Heck S, Jelovina D, Perry C, Zinchenko K, Lucchese R, Wörner HJ. Attosecond spectroscopy of size-resolved water clusters. *Nature*. 2022;609:507–511.
18. Kienberger R, Goulielmakis E, Uiberacker M, Baltuska A, Yakovlev V, Bammer F, Scrinzi A, Westerwalbesloh T, Kleineberg U, Heinzmann U, et al. Atomic transient recorder. *Nature*. 2004;427:817–821.
19. Ossiander M, Riemensberger J, Neppl S, Mittermair M, Schäffer M, Duensing A, Wagner MS, Heider R, Wurzer M, Gerl M, et al. Absolute timing of the photoelectric effect. *Nature*. 2018;561:374–377.
20. Wang L, Wang X, Xiao F, Wang J, Tao W, Zhang D, Zhao Z. Chirp compensation for generating ultrashort attosecond pulses with 800-nm few-cycle pulses. *Chin Phys Lett*. 2023;40(11):Article 113201.
21. Ferray M, L'Huillier A, Li XF, Lompre LA, Mainfray G, Manus C. Multiple-harmonic conversion of 1064 nm radiation in rare gases. *J Phys B Atomic Mol Phys*. 1988;21(3):L31.
22. Sansone G, Benedetti E, Calegari F, Vozzi C, Avaldi L, Flammini R, Poletto L, Villoresi P, Altucci C, Velotta R, et al. Isolated single-cycle attosecond pulses. *Science*. 2006;314(5798):443–446.
23. Goulielmakis E, Schultze M, Hofstetter M, Yakovlev VS, Gagnon J, Uiberacker M, Aquila AL, Gullikson EM, Attwood DT, Kienberger R, et al. Single-cycle nonlinear optics. *Science*. 2008;320(5883):1614–1617.
24. Gaumnitz T, Jain A, Pertot Y, Huppert M, Jordan I, Ardana-Lamas F, Wörner HJ. Streaking of 43-attosecond soft-X-ray pulses generated by a passively CEP-stable mid-infrared driver. *Opt Express*. 2017;25(22):27506–27518.
25. Li J, Ren X, Yin Y, Zhao K, Chew A, Cheng Y, Cunningham E, Wang Y, Hu S, Wu Y, et al. 53-attosecond X-ray pulses reach the carbon K-edge. *Nat Commun*. 2017;8:186.
26. Ren X, Mach LH, Yin Y, Wang Y, Chang Z. Generation of 1 kHz, 23 mJ, 88 fs, 25 μm pulses from a Cr^{2+}:ZnSe chirped pulse amplifier. *Opt Lett*. 2018;43(14):3381–3384.
27. Wu Y, Zhou F, Larsen EW, Zhuang F, Yin Y, Chang Z. Generation of few-cycle multi-millijoule 2.5 μm pulses from a single-stage Cr2+:ZnSe amplifier. *Sci Rep*. 2020;10(1):7775.
28. Le A-T, Wei H, Jin C, Tuoc VN, Morishita T, Lin CD. Universality of returning electron wave packet in high-order harmonic generation with midinfrared laser pulses. *Phys Rev Lett*. 2014;113(3):Article 033001.
29. Emelina AS, Emelin MY, Ryabikin MY. Wavelength scaling laws for high-order harmonic yield from atoms driven by mid- and long-wave infrared laser fields. *J Opt Soc Am B*. 2019;36(11):3236–3245.
30. Zhang Q, Zhao K, Chang Z. Attosecond extreme ultraviolet supercontinuum. In: *The supercontinuum laser source*. New York (NY): Springer; 2016. pp. 337–370.
31. Oguri K, Mashiko H, Ogawa T, Hanada Y, Nakano H, Gotoh H. Sub-50-as isolated extreme ultraviolet continua generated by 1.6-cycle near-infrared pulse combined with double optical gating scheme. *Appl Phys Lett*. 2018;112: Article 181105.
32. Mashiko H, Oguri K, Sogawa T, Mashiko H, Oguri K, Sogawa T. Attosecond pulse generation in carbon K-edge region (284 eV) with sub-250 μJ driving laser using generalized double optical gating method. *Appl Phys Lett*. 2013;102(17):171111.
33. Mashiko H, Gilbertson S, Chini M, Feng X, Yun C, Wang H, Khan SD, Chen S, Chang Z. Extreme ultraviolet supercontinua supporting pulse durations of less than one atomic unit of time. *Opt Lett*. 2009;34(21):3337–3339.

34. Feng X, Gilbertson S, Mashiko H, Wang H, Khan SD, Chini M, Wu Y, Zhao K, Chang Z. Generation of isolated attosecond pulses with 20 to 28 femtosecond lasers. *Phys Rev Lett*. 2009;103(18):Article 183901.
35. Chini M, Zhao K, Chang Z. The generation, characterization and applications of broadband isolated attosecond pulses. *Nat Photonics*. 2014;8:178–186.
36. Gilbertson S, Khan SD, Wu Y, Chini M, Chang Z. Isolated attosecond pulse generation without the need to stabilize the carrier-envelope phase of driving lasers. *Phys Rev Lett*. 2010;105(9):Article 093902.
37. Wang X, Wang L, Xiao F, Zhang D, Lue Z, Yuan J, Zhao Z. Generation of 88 as isolated attosecond pulses with double optical gating. *Chin Phys Lett*. 2020;37(2):Article 023201.
38. Thomann I, Bahabad A, Liu X, Trebino R, Murnane MM, Kapteyn HC. Characterizing isolated attosecond pulses from hollow-core waveguides using multi-cycle driving pulses. *Opt Express*. 2009;17(6):4611–4633.
39. Wang J, Xiao F, Wang L, Tao W, Wang X, Zhao Z. Fast phase retrieval for broadband attosecond pulse characterization. *Opt Express*. 2023;31(26):43224–43233.
40. Kretschmar M, Svirplys E, Volkov M, Witting T, Nagy T, Vrakking MJJ, Schütte B. Compact realization of all-attosecond pump-probe spectroscopy. *Sci Adv*. 2024;10(8):eadk9605.
41. Mairesse Y, Quéré F. Frequency-resolved optical gating for complete reconstruction of attosecond bursts. *Phys Rev A*. 2005;71:Article 011401.
42. Chini M, Gilbertson S, Khan SD, Chang Z. Characterizing ultrabroadband attosecond lasers. *Opt Express*. 2010;18(12):13006–13016.
43. Lucchini M, Brügmann MH, Ludwig A, Gallmann L, Keller U, Feurer T. Ptychographic reconstruction of attosecond pulses. *Opt Express*. 2015;23(23):29502–29513.
44. Keathley PD, Bhardwaj S, Moses J, Laurent G, Kärtner FX. Volkov transform generalized projection algorithm for attosecond pulse characterization. *New J Phys*. 2016;18: Article 073009.
45. White J, Chang Z. Attosecond streaking phase retrieval with neural network. *Opt Express*. 2019;27(4):4799–4807.
46. Zhao X, Wang S-J, Yu W-W, Wei H, Wei C, Wang B, Chen J, Lin CD. Metrology of time-domain soft x-ray attosecond pulses and reevaluation of pulse durations of three recent experiments. *Phys Rev Appl*. 2020;13(3):Article 034043.
47. Brunner C, Duensing A, Schröder C, Mittermair M, Golkov V, Pollanka M, Cremers D, Kienberger R. Deep learning in attosecond metrology. *Opt Express*. 2022;30(9):15669–15684.
48. Dolso GL, Inzani G, Di Palo N, Moio B, Medeghini F, Borrego-Varillas R, Nisoli M, Lucchini M. Versatile and robust reconstruction of extreme-ultraviolet pulses down to the attosecond regime. *APL Photonics*. 2023;8:Article 076101.
49. Kim KT, Kim CM, Baik MG, Umesh G, Nam CH. Compression of harmonic pulses by using material dispersion. *Appl Phys B Lasers Opt*. 2004;79:563–567.
50. Ko DH, Kim KT, Nam CH. Attosecond-chirp compensation with material dispersion to produce near transform-limited attosecond pulses. *J Phys B Atomic Mol Phys*. 2012;45: Article 074015.
51. Chang Z. Attosecond chirp compensation in water window by plasma dispersion. *Opt Express*. 2018;26(25):33238–33244.
52. Chang Z. Compensating chirp of attosecond X-ray pulses by a neutral hydrogen gas. *OSA Contin*. 2019;2(2):314–319.
53. Chini M, Mashiko H, Wang H, Chen S, Yun C, Scott S, Gilbertson S, Chang Z. Delay control in attosecond pump-probe experiments. *Opt Express*. 2009;17(24):21459–21464.
54. Gao J, Wu J, Lou Z, Yang F, Qian J, Peng Y, Leng Y, Zheng Y, Zeng Z, Li R. High-order harmonic generation in an x-ray range from laser-induced multivalent ions of noble gas. *Optica*. 2022;9(9):1003–1008.
55. Ye P, Gulyás Oldal L, Csizmadia T, Filus Z, Grósz T, Jójárt P, Seres I, Bengery Z, Gilicze B, Kahaly S, et al. High-flux 100 kHz attosecond pulse source driven by a high-average power annular laser beam. *Ultrafast Sci*. 2022;2022:9823783.
56. Xiao F, Fan X, Wang L, Zhang D, Wu J, Wang X, Zhao Z. Generation of intense sub-10 fs pulses at 385nm. *Chin Phys Lett*. 2020;37(11):Article 114202.